Journal of Luminescence 133 (2013) 157–161

Contents lists available at SciVerse ScienceDirect

Journal of Luminescence

journal homepage: www.elsevier.com/locate/jlumin

Coherent phonon generation in semiconducting single-walled carbon nanotubes using a few-cycle pulse laser

Takayoshi Kobayashi [a,b,c,d,e,*], Zhaogang Nie [a,b], Juan Du [a,b,c], Hiromichi Kataura [f], Youichi Sakakibara [g], Yasumitsu Miyata [h]

[a] Advanced Ultrafast Laser Research Center, University of Electro-Communications, 1-5-1 Chofugaoka, Chofu, Tokyo 182-8585, Japan
[b] JST, CREST, K's Gobancho, 7, Gobancho, Chiyoda-ku, Tokyo, 102-0076, Japan
[c] Core Research for Evolutional Science and Technology, Japan Science and Technology Agency, 4-1-8 Honcho, Kawaguchi, Saitama 332-0012, Japan
[d] Department of Electrophysics, National Chiao-Tung University, Hsinchu 30010, Taiwan
[e] Institute of Laser Engineering, Osaka University, 2-6 Yamada-oka, Suita, Osaka 565-0871, Japan
[f] Nanosystem Research Institute, AIST, Higashi 1-1-1, Tsukuba, Ibaraki 305-8562, Japan
[g] Photonics Research Institute, AIST, Higashi 1-1-1, Tsukuba, Ibaraki 305-8562, Japan
[h] Department of Chemistry, Nagoya University, Furo-cho, Chikusa-ku, Nagoya, 464-8601, Japan

ARTICLE INFO

Available online 13 December 2011

Keywords:
Single-walled carbon nanotubes
Coherent phonon spectroscopy
Few-cycle pulse laser

ABSTRACT

Coherent phonon dynamics in single-walled carbon nanotubes with several chiralities is investigated by 7.1-fs pump–probe experiments. Vibrational wave-packets corresponding to the radial breathing mode (RBM) and *G* mode can be detected for four chiral systems, (6,4), (6,5), (7,5) and (8,3). Coherent phonon generation of RBMs is in-depth studied by analyzing the probe photon energy dependent amplitude profiles, which indicates that the real and imaginary parts of the third-order susceptibility can both contribute to the modulation of the probed difference absorbance.

1. Introduction

Single-walled carbon nanotubes (SWNTs), with unique mechanical, electronic and optical properties, enable groundbreaking applications in nanoelectronics and photonics. Their one-dimensionality provides a playground for studying the dynamics of confined electrons and phonons and their interplay [1–4]. Recently, many efforts have been made to investigate the coherent lattice vibrations (phonon) in SWNTs by coherent phonon (CP) spectroscopy via femtosecond pump–probe techniques [5–14]. Extensive studies were made on the mechanism of the spectroscopic appearance of the CP generation. It is argued that the coupling of the phonon modes to the electronic structure resulting in the modulations of the difference absorbance [5–14]. The vibrations of radial breathing mode (RBM) was explained as ultrafast modulations of optical constant at frequency ω_{RBM} due to band gap (E_g) oscillations induced by the change of the diameter Φ_d ($E_g \propto 1/\Phi_d$). It is claimed that the photon energy dependence of the CP signal shows a derivative-like behavior [6–8]. However, as described later discussion in the present paper the agreement of the probe wavelength dependence of the RBM amplitude is not good enough to support the explanation. The problem in the previous papers to discuss the origin of the real-time vibration (phonon) signal associated with the modulation of the electronic (excitonic) transitions based on the experiments was caused by relatively smaller number of probe energies, which made argument on the mechanism ambiguous due to the limited the precise acquisition of complete dependence signal of vibrational amplitudes on probe photon energy.

Here, we report on the use of resonant 7.1-fs visible pulses to generate and detect CPs in SWNTs. We probed 128 different wavelengths simultaneously by using a detection system composed of a polychromator and a multichannel lock-in amplifier. We separately observed four semiconducting chiral systems without ambiguity, and obtained abundant date points of the probe photon energy dependence of the phonon amplitudes for RBMs, which allow an in-depth study of the origin of the CP generation in SWNTs further. Since the process of pump–probe experiment is the third-order nonlinear process, the effects of the real and imaginary parts of the third-order susceptibility on the modulation of the probed absorbance change are fully discussed. The probe photon energy dependent amplitude profiles are discussed in relation with the mechanism of the modulation of excitonic transition probability.

* Corresponding author at: Advanced Ultrafast Laser Research Center, University of Electro-Communications, 1-5-1 Chofugaoka, Chofu, Tokyo 182-8585, Japan. Tel.: +81 42 443 5846.
E-mail address: kobayashi@ils.uec.ac.jp (T. Kobayashi).

0022-2313/$ - see front matter © 2011 Elsevier B.V. All rights reserved.
doi:10.1016/j.jlumin.2011.12.021

2. Experimental details

The SWNT sample was prepared by CoMoCat method [15–17]. The pump and probe light sources were from the non-collinear parametric amplifier (NOPA). The pump source of this system is a commercially supplied regenerative amplifier (Spectra Physics, Spitfire). The central wavelength, pulse duration, power of the output, and repetition rate of this amplifier were 800 nm, 50 fs, 740 mW, and 5 kHz, respectively. With the use of a compression system composed of a pair of prisms and a pair of chirped mirrors, the system supported a pulse with pulse duration of 7.1 fs with constant spectral phase, indicating that the pulses are nearly Fourier-transform limited. The energy of the pump is ~32 nJ. The probe pulse energy is five times weaker than the pump pulse.

The polarization of the pump and probe beams are parallel to each other. In the pump–probe experiment, signal was spectrally dispersed with a polychromator (JASCO, M25-TP) over 128 photon energies (wavelengths) from 1.71 to 2.36 eV (722 to 524 nm). It was detected by 128 sets of avalanche photodiodes and lock-in amplifiers with a reference from an optical chopper intersecting the pump pulse at the 2.5-kHz repetition rate. Details about our 7.1-fs pump-probe experimental setup and working principle of the techniques are described elsewhere [18,19].

3. Results and discussion

3.1. Stationary absorption spectrum of the sample and laser spectrum

Fig. 1(a) shows the stationary absorption spectrum of SWNTs with the relevant chirality assignments [15]. The assignments of some absorption bands might be uncertain since they might be shared by more than one type of tubes because of their finite spectral widths. The broadband visible laser spectrum is resonant with the second exciton transitions (E_{22}) of the tubes in 1.71 – 2.36 eV range. For the analysis of the real-time data in the latter part of this paper, the absorption spectrum was fitted by the sum of five dominant Voigt functions, which are the convolution of the Gaussian and Lorentzian functions at 2.17 eV, 2.08 eV, 1.91 eV 1.84 eV and 1.78 eV corresponding to (6,5), (6,4), (7,5), (8,3), and (9,1) tubes, respectively. The properties of tubes (9,1) will not be discussed here due to its weak absorption. The *absorbed laser spectrum* for different chiralities is also calculated, as shown in Fig. 1(b), which is defined latter by the difference in the spectrum between the probe light before and after passing through the sample. The application of the absorbed spectrum will be further discussed later for successful fitting the experimental probe photon energy dependent amplitude profiles.

3.2. Two-dimensional (2D) real-time spectra and exact chirality assignment

Two-dimensional (2D) difference absorption ΔA (E_{pr}, t) was represented in Fig. 2(a), showing clear oscillations in ΔA amplitude with time as stripe-like structures. The Fourier transform (FT) of the ΔA time traces is shown in Fig. 2(b). This plot identifies two well-known dominant vibrational modes [5]: RBMs at ~250–350 cm^{-1} (~95–133 fs) and G modes at ~1587 cm^{-1} (~21 fs), generated by impulsive excitation with pulse duration (7.1 fs) much smaller than vibrational periods. The vibrations with frequencies from 360 cm^{-1} to 1525 cm^{-1} are disregarded here since they are too weak to be resolved. The probe photon energy dependence of vibrational amplitudes is well displayed for RBMs. According to the results previously reported, the four dominant symmetric double-peak structures, as indicated by the two-way

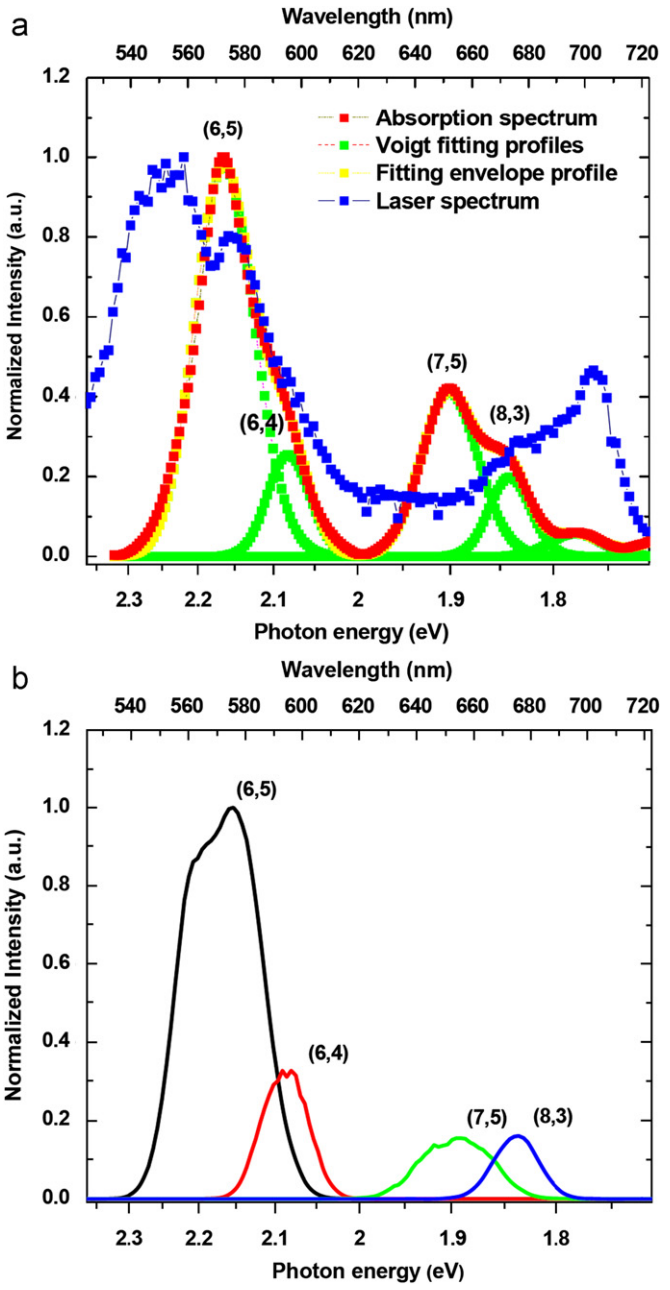

Fig. 1. (a) Laser spectrum (blue line) and stationary visible absorption spectrum of SWNTs (red line) after subtracting the weak background and its Voigt fitting profiles (green lines), illustrating individual E_{22} absorption components in 1.7 – 2.4 eV spectral range. The chirality assignments are shown together. (b) Absorbed spectra, defined by the difference in the spectrum between the probe light before and after passing thorough the sample, for different chiralities. (For interpretation of the references to color in this figure legend, the reader is referred to the web version of this article.)

arrows, should follow the first-derivative of electronic resonances [6–8]. The middle dip for each structure should correspond to the E_{22} transitions for relevant chiralities since the oscillation becomes minimal at resonance. And then, bearing in mind that the Raman shifts for different RBMs should theoretically correspond to their phonon frequencies in the CP spectra, chirality assignments for four chiralities (6,4), (6,5), (7,5), and (8,3) can be achieved exactly, since only these specific type of tubes can fulfill the above frequency and resonance conditions simultaneously for each mode. For the G mode vibrations, however, the amplitude profiles overlap together for different chiralities and can not be

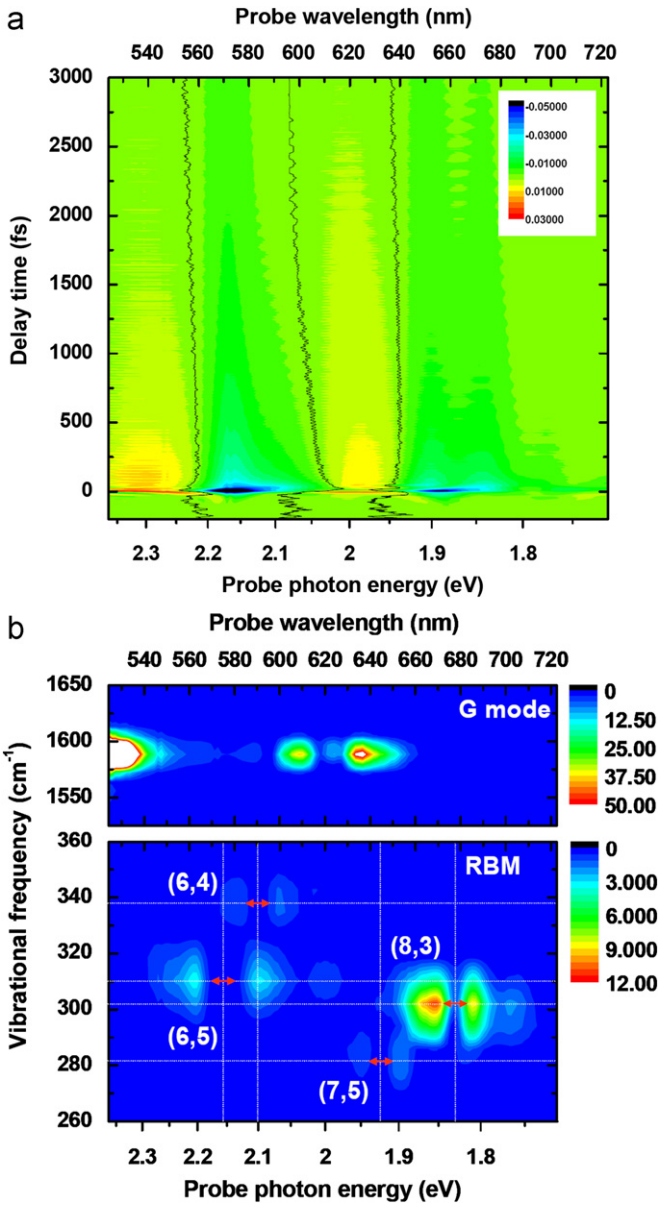

Fig. 2. (a) 2D display of $\Delta A\,(E_{pr}, t)$ as functions of probe photon energy, E_{pr}, and probe delay time, t. The black curves are related to the zero-change lines in the absorbance ($\Delta A=0$). (b) 2D coherent phonon spectra in the spectral range of 1.7 – 2.4 eV. The chirality assignments of RBMs are shown together. The dotted crisscrossing lines show the relevant vibrational frequencies and resonance energies corresponding to RBMs. The two-way arrows indicate the double-peak structure in the amplitude profile of RBMs.

distinguished because the axial G^+-mode is known to be insensitive to the diameter and chirality of SWNTs. [5]

3.3. Probe photon energy dependent amplitude profiles

In previous reports studying the CPs in SWNTs, the probe photon energy (or wavelength) dependence of the RBM amplitudes was compared with the first-derivative of the relevant absorptions and it was claimed that the close resemblance between the amplitude profiles to the derivative is the verification of the wavepacket motion [6–8]. However, the results of fitting analyses are far from sufficient agreement and the exact mechanism of the wavepacket motion has not been investigated in detail.

It is well known that the wavefunction of the electronic state can be factorized into the electronic part and vibrational part under the Born–Oppenheimer approximation, $\Psi(Q,q)=\Phi(Q,q)\chi(Q)$, where $\Phi(Q,q)$ and $\chi(Q)$ represent wavefunctions of the electrons and nuclei, respectively. Usually Franck–Condon approximation given below is good enough to formulate the time dependence of the transition probability with the frequency of CP in case without anharmonicity. Following the Franck–Condon principle, dipole transition under the Condon approximation is given by

$$\begin{aligned}&\langle\Psi_1(Q,q)|eq|\Psi_2(Q,q)\rangle_{Q,q}\\&\quad\approx\langle\!\langle\Phi_1(Q,q)|eq|\Phi_2(Q,q)\rangle_q\chi(Q)|\chi(Q)\rangle_Q\\&\quad\approx\langle\Phi_1(Q_0,q)|eq|\Phi_2(Q_0,q)\rangle_q\langle\chi(Q)|\chi(Q)\rangle_Q\end{aligned}\tag{1}$$

The Franck–Condon factor, $\langle\chi(Q)|\chi(Q)\rangle_Q=\langle\Sigma_i c_i\chi_i(Q)|\Sigma_j c_j\chi_j(Q)\rangle_Q$, gives the time dependence of the transition probability with the frequency of CP in case without anharmonicity. Then the change of the transition probability due to the wave-packet motion cannot be simply described by the smooth motion of the wave-packet along the corresponding normal mode [20]. The observed spectral shift described by the derivative type dependence caused by small smooth shift is due to phase modulation of the probe light by the wavepacket motion. This is in principle related to the real part of the third-order susceptibility on the absorption difference. In this case at fixed probe energy, this effect translates into an amplitude modulation via a probe pulse spectral change induced by the cross-phase modulation mechanism [21,22]. This mechanism in effect results from the refractive index change caused by the deformation of the lattice/molecular configuration during the coherent lattice/molecular vibrations. The refractive index change then introduces the linear shift of the probe energy. Therefore the signal can be simply approximated with the spectral (linear) shift of the probe pulse induced by cross-phase modulation, and the probe energy dependence of phonon amplitude follows the first-derivative of the electronic resonance (denoted by derivative-type hereafter), in consistent with the first-derivative analysis as reported recently [6–8].

The probe photon energy dependence of vibrational amplitude of RBMs for three chiralities is plotted in Fig. 3(a–c), which is obtained by cutting through the 2D FT power spectra at the relevant central frequencies and then taking the square roots. We firstly performed the fitting of the amplitude profiles (black lines) with the first-derivative of the relevant absorption components (gray lines) for different chiralities, as shown in the top panels in Fig. 3. Each of the corresponding absorption components is obtained by the spectral deconvolution of the stationary absorption spectrum by Voigt fitting in Fig. 1. Similar to the results reported in literatures [8], the typical two-peak structure, which is expected by the first-derivative dependence, cannot be well fitted, even after slightly modifying the absorption components by second-derivative to improve the disagreement between the absorption spectra and the fitted spectra. There are always substantial deviations in the valley-dip positions in the spectra of the probe photon energy dependence and the first-derivative of the absorptions, and the line shapes between the derivatives and the amplitudes cannot agree well with each other. A similar phenomenon was also reported for chirality (6,5) highly enriched samples when the amplitude dependence was fitted by first-derivative profile [8]. Considering that the line-shape of the laser spectrum can affect the actual acquisition of laser energy, we further compared the amplitudes with the derivative of the *absorbed laser spectrum* (red lines), defined later as the spectral distribution of the laser photon absorbed by the sample. In this case, it seems the line-shape fitting is improved, but large deviations in the valley-dip positions in the probe dependent

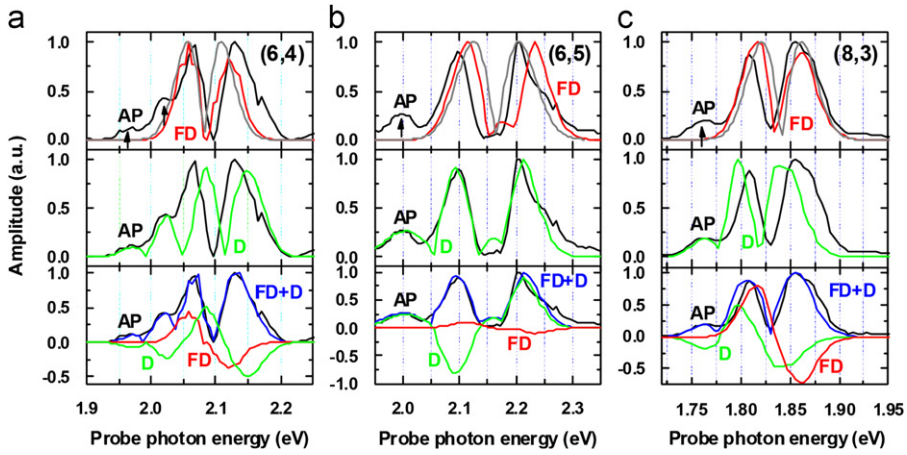

Fig. 3. Probe photon energy dependent RBM amplitudes (AP, black lines) for (a) (6,4), (b) (6,5) and (c) (8,3) tubes, fitted with the first-derivative type (FD, gray lines), the absorbed laser spectra (FD, red lines), the difference-type only (D, green lines), and the sum of FD and D (FD+D, blue lines) with relevant contributions, respectively. The arrows indicate the side bands. In the bottom columns the original FD (red lines) and D (green lines) lines are plotted together before taking absolute value to show their corresponding contributions to the vibrational amplitudes. The amplitude profile of (7,5) is not studied here since it is very weak. (For interpretation of the references to color in this figure legend, the reader is referred to the web version of this article.)

spectra remain substantially large. Especially, the side bands, as indicated by the arrows in Fig. 3, are already outside of the range of the resonance energy distributions. They cannot be well fitted in any case, as just inferred from first-derivative calculation. More interestingly, we found the energy difference between the side bands and each one of the peaks in the double-band structure is always of an integral number of the relative RBM frequencies. This observation brought us to further take into account the Raman interaction contributions between the probe pulse and the coherent vibrations [21,22], as discussed below.

Because of the Kramers–Kronig relations, the effect of the imaginary part (denoted by difference-type hereafter) is also taking place, which is essentially the Raman gain/loss process induced by the energy exchange between the CPs and the probe optical field, according to the relation, $\Delta A(\omega,\tau)\propto -\mathrm{Im}[P^{(3)}(\omega,\tau)/E_{\mathrm{probe}}(\omega,\tau)]$, where $P^{(3)}(\omega,\tau)$ is the nonlinear polarization induced by pump and probe pulses, and $E_{\mathrm{probe}}(\omega,\tau)$ is the electronic field of the optical probe pulse. In this process, the probe optical field is alternately deamplified and amplified in corresponding transitions depending on the phase change of the vibrations. So the FT power spectral shapes are considered to depend on the spectral distribution of the laser photons absorbed by the sample. For quantitative discussion, the probe photon energy dependence of vibrational amplitude $V(\omega_{\mathrm{probe}})$ can be phenomenologically described by

$$V(\omega_{\mathrm{probe}}) = C_S\left|a(\omega_{\mathrm{probe}}) - a(\omega_{\mathrm{probe}}-\omega_\nu)\right| \tag{2.1a}$$

$$V_{AS}(\omega_{\mathrm{probe}}) = C_{AS}\left|a(\omega_{\mathrm{probe}}) - a(\omega_{\mathrm{probe}}+\omega_\nu)\right| \tag{2.1b}$$

$$a(\omega_{\mathrm{probe}}) = L(\omega_{\mathrm{probe}})(1-10^{-A(\omega_{\mathrm{probe}})}), \tag{2.2}$$

where C_S and C_{AS} are proportionality constant, corresponding to the cases of pump/Stokes and pump/anti-Stokes interactions, respectively, $a(\omega_{\mathrm{probe}})$ is the absorbed laser spectrum at ω_{probe}, the optical frequency of probe light, ω_ν is the molecular vibration frequency, $L(\omega_{\mathrm{probe}})$ is the laser spectrum and $A(\omega_{\mathrm{probe}})$ is the absorbance of the sample at ω_{probe}. The interaction between the CP and probe optical field can be between the first (anti-) Stokes beam and the absorbed beam and also can be between higher-order (anti-) Stokes beams. Based on the analysis above, the amplitude profiles can be fitted with the absolute difference between the absorbed photon energy distribution and the distribution shifted by the amount of vibration frequency (denoted by difference-type). The difference-type fitting are displayed in the middle panels of Fig. 3. In the fitting the π-phase jump between the neighboring contributions was taken into account. Including the Raman contributions the fitting is obviously improved very much, except for those of the valley-dip positions, which thus means the good fitting cannot be achieved only with the mechanism of either difference-type or derivative-type mechanism. Considering that the effect of the real part can play roles simultaneously with the imaginary part, we continued to perform the fitting with the sum contributions of the two types of mechanisms with adjustable parameters of relative amount of contributions. As shown in the bottom panels of Fig. 3, we finally achieved the fitting perfectly. The sum contributions (blue lines) of the two type of mechanisms for different RBMs is demonstrated by adjusting the parameters of the relative amount of contributions from different fitting origins, derivative type (red lines) and difference-type (green lines), before taking absolute values. Thus, in contrast to the results reported in literatures recently [6–8], in which the intensity of the RBM mode was poorly fitted to the first-derivative of corresponding absorption of the chiral species due to spectral change associated with the wavepacket motion, the fitting results here indicates that the real and the imaginary parts of the third-order susceptibility can both contribute to the modulation of the absorbance change, and the latter is also a dominant contributor to the modulation of the difference absorbance.

4. Conclusions

We separately observed four RBM systems without ambiguity in CoMoCat grown SWNTs by using a 7.1 fs broadband visible pulse and an ultra high-sensitive detection system. The amplitude profiles of RBMs can be fitted perfectly by the sum of the first-derivative of the absorption due to the real part of the susceptibility and the difference absorption due to the imaginary part induced by a Raman gain/loss process with adjustable contributions. The imaginary part can also be a dominant contributor in the modulation of difference absorbance. The Raman process is explained in terms of the energy exchange between coherent phonons and probe optical field.

References

[1] S. Iijima, Nature (London) 354 (1991) 56.
[2] M.S. Dresselhaus, G. Dresselhaus, P. Avouris (Eds.), Carbon Nanotubes: Synthesis, Structure, Properties and Applications, Springer, Berlin, 2001.

[3] M. Dresselhaus, Carbon nanotubes: synthesis, structure, properties R. Saito, G. Dresselhaus, and M. Dresselhaus, in Physical Properties of Carbon Nanotubes (World Scientific, Singapore, 2003).
[4] P. Harris, in: Carbon Nanotubes and Related Structures: New Materials for the Twenty-First Century (Cambridge University Press, Cambridge, England, 1999).
[5] A. Gambetta, C. Manzoni, E. Menna, M. Meneghetti, G. Cerullo, G. Lanzani, S. Tretiak, A. Piryatinski, A. Saxena, R.L. Martin, A.R. Bishop, Nat. Phys. 2 (2006) 515.
[6] Y.-S. Lim, K.-J. Yee, J.H. Kim, E.H. Hároz, J. Shaver, J. Kono, S.K. Doorn, R.H. Hauge, R.E. Smalley, Nano Lett. 6 (2006) 2696.
[7] J.-H. Kim, K.-J. Han, N.-J. Kim, K.-J. Yee, Y.-S. Lim, G.D. Sanders, C.J. Stanton, L.G. Booshehri, E.H. Hároz, J. Kono, Phys. Rev. Lett. 102 (2009) 037402.
[8] Larry Lüer, Christoph Gadermaier, Jared Crochet, Tobias Hertel, Daniele Brida, Guglielmo Lanzani, Phys. Rev. Lett. 102 (2009) 127401.
[9] G.D. Sanders, C.J. Stanton, J.-H. Kim, K.-J. Yee, Y.-S. Lim, E.H. Hároz, L.G. Booshehri, J. Kono, R. Saito, Phys. Rev. B. 79 (2009) 205434.
[10] K. Kato, K. Ishioka, M. Kitajima, J. Tang, R. Saito, H. Petek, Nano Lett. 8 (2008) 3102.
[11] Kotaro Makino, Atsushi Hirano, Kentaro Shiraki, Yutaka Maeda, Muneaki Hase, Phys. Rev. B. 80 (2009) 245428.
[12] Yong-Sik Lim, Jae-Geum Ahn, Ji-Hee Kim, Ki-Ju Yee, Taiha Joo, Sung-Hoon Baik, Erik H. Hàroz, Layla G. Booshehri, Junichiro Kono, ACS Nano 4 (2010) 3222.
[13] Jigang Wang, Matt W. Graham, Yingzhong Ma, Graham R. Fleming, Robert A. Kaindl, Phys. Rev. Lett. 104 (2010) 177401.
[14] Zipeng Zhu, Jared Crochet, Michael S. Arnold, Mark C. Hersam, Hendrik Ulbricht, Daniel Resasco, Tobias Hertel, J. Phys. Chem. C 111 (2007) 3831.
[15] Michael S. Arnold, Samuel I. Stupp, Mark C. Hersam, Nano Lett. 5 (2005) 713.
[16] Sergei M. Bachilo, Leandro Balzano, Jose E. Herrera, Francisco Pompeo, Daniel E. Resasco, R. Bruce Weisman, J. Am. Chem. Soc. 125 (2003) 11186.
[17] Yasumitsu Miyata, Kazuhiro Yanagi, Yutaka Maniwa, Takeshi Tanaka, Hiromichi Kataura, J. Phys. Chem. C 112 (2008) 15997.
[18] T. Kobayashi, M. Yoshizawa, U. Stamm, M. Taiji, M. Hasegawa, J. Opt. Soc. Am. B 7 (1990) 1558.
[19] A. Baltuska, T. Fuji, T. Kobayashi, Opt. Lett. 27 (2002) 306.
[20] T. Kobayashi, Z. Wang, Izumi Iwakura, New J. Phys. 10 (2008) 065009.
[21] N. Ishii, E. Tokunaga, S. Adachi, T. Kimura, H. Matsuda, T. Kobayashi, Phys. Rev. A. 70 (2004) 023811.
[22] T. Kobayashi, Z. Wang, IEEE J. Quant. Electron 44 (2008) 1232.